MinMax-CAM: Improving Focus of CAM-based Visualization Techniques in Multi-label Problems

Lucas David[a], Helio Pedrini[b] and Zanoni Dias[c]
Institute of Computing, University of Campinas, Campinas, Brazil

Keywords: Computer Vision, Multi-label, Explainable Artificial Intelligence.

Abstract: The Class Activation Map (CAM) technique (and derivations thereof) has been broadly used in the literature to inspect the decision process of Convolutional Neural Networks (CNNs) in classification problems. However, most studies have focused on maximizing the coherence between the visualization map and the position, shape and sizes of a single object of interest, and little is known about the performance of visualization techniques in scenarios where multiple objects of different labels coexist. In this work, we conduct a series of tests that aim to evaluate the efficacy of CAM techniques over distinct multi-label sets. We find that techniques that were developed with single-label classification in mind (such as Grad-CAM, Grad-CAM++ and Score-CAM) will often produce diffuse visualization maps in multi-label scenarios, overstepping the boundaries of their explaining objects onto different labels. We propose a generalization of CAM technique, based on multi-label activation maximization/minimization to create more accurate activation maps. Finally, we present a regularization strategy that encourages sparse positive weights in the classifying layer, producing cleaner activation maps and better multi-label classification scores.

1 INTRODUCTION

Convolutional Neural Networks (CNNs) have become paramount in the solution of many modern computer vision problems, such as image classification (Rawat and Wang, 2017), object detection (Dhillon and Verma, 2020) and localization, image segmentation (Minaee et al., 2021) and pose estimation (Wei et al., 2016). Additionally, CNNs have also shown great promise when working with unstructured data from multiple non-imagery domains, such as audio processing (Pons et al., 2017), text classification (Yao et al., 2019) and text-to-speech (Tachibana et al., 2018), with few changes in their original formulation.

In spite of their unquestionable efficacy, their massive composition of operations degrades overall interpretability, rendering “black box” models. As CNNs gradually permeate into many real-world systems, impacting different demographics, the necessity for explaining and accountability becomes urgent.

While the construction of interpretable models is desirable as a general rule, as it facilitates the identification of failure modes while hinting strategies to fix them (Selvaraju et al., 2017), it is also an essential component in building trust from the general public towards this technology (Huff et al., 2021).

In this work, we attempt to evaluate and extend visualization and visual explaining techniques based on Class Activation Maps (CAMs) onto a multi-label scenario, in which analysis can be considerably more challenging (Tarekegn et al., 2021). The main contributions of this work are the following:

1. We propose a thoroughly analysis of popular visualization techniques in the literature over a distinct set of multi-label problems, evaluating their results according to the offered coverage over objects belonging to the label of interest, as well as the containment within objects of said label.
2. We propose a modification to CAM-based methods that combines gradient information from multiple labels within a single input image. We demonstrate that our approach presents better scores and cleaner visualization maps than other methods over distinct datasets and architectures.
3. We present a regularization strategy that encourages networks to associate each learned label with a distinct set of patterns, resulting in better separation of concepts and producing cleaner CAM visualizations, with better scores.

[a] https://orcid.org/0000-0002-8793-7300
[b] https://orcid.org/0000-0003-0125-630X
[c] https://orcid.org/0000-0003-3333-6822

David, L., Pedrini, H. and Dias, Z.
MinMax-CAM: Improving Focus of CAM-based Visualization Techniques in Multi-label Problems.
DOI: 10.5220/0010807800003124
In *Proceedings of the 17th International Joint Conference on Computer Vision, Imaging and Computer Graphics Theory and Applications (VISIGRAPP 2022) - Volume 4: VISAPP*, pages 106-117
ISBN: 978-989-758-555-5; ISSN: 2184-4321

The remaining of this work is organized as follows. Section 2 summarizes the explaining methods currently used in literature. Section 3 describes our approach in detail, while Section 4 presents the experimental setup used to evaluate our strategy, the datasets and network architectures employed. We discuss our main results in Section 5 and present a regularization strategy to improve them in Section 6. Finally, we conclude the paper in Section 7 by remarking our results and proposing future work.

2 RELATED WORK

In the context of computer vision, CNNs are often inspected with the aid of visual explanation strategies, in which important regions that most contribute to the answer provided by the aforementioned model are somehow indicated to the user. Early work in this vein, namely gradient-based saliency methods (Simonyan et al., 2014), attempted to highlight regions of importance by back-propagating the gradient information from the last layers to the input signal, forming a saliency map that described which pixels had most overall contribution to the score estimated network's decision process.

Sub-sequentially, multiple variations of the gradient-based saliency strategy have been proposed in an attempt to improve the quality of the visualization maps. Instances of these studies are Guided Backpropagation (Springenberg et al., 2015), which filters out the negative backpropagated gradients; SmoothGrad (Smilkov et al., 2017), which averages gradient maps obtained from multiple noisy copies of a single input image; and FullGrad (Srinivas and Fleuret, 2019), which combines the bias unit partial contributions with the saliency information in order to create a "full gradient" visualization.

Notwithstanding their precision on identifying salient regions, many of these methods will ultimately fail to identify cohesive regions of the image that relate to a specific class of interest. In this vein, Adebayo et al. proposed to evaluate saliency methods considering *Model Parameter Randomization* and *Data Randomization* (Adebayo et al., 2018). In the former, weights from layers would be progressively (or individually) randomized, from top to bottom, and the effect over the saliency map produced by each method would be observed. In the latter, labels would be permuted in the training set, forcing the network to memorize the randomized labels. The authors found that some of the saliency methods (such as Guided Backpropagation and Guided-CAM) were unaffected by the randomization of labels and weights of the top layers, indicating that these methods approximated the behavior of edge detectors, as they were invariant to class information and highly dependent on low-level features.

Class Activation Mapping (CAM) can be used to circumvent the lack of sensibility to class (Zhou et al., 2016). Although limited to relatively simple CNN architectures, comprising convolutions, *Global Average Pooling* (GAP) and dense linear layers, this technique resulted in visualization maps with clear class distinctions. It consisted of feed-forwarding an input image x over all convolutional layers of a CNN f and obtaining the positional activation signal $A^k = [a^k_{ij}]_{H\times W}$ for the k-th kernel in the last convolutional layer. If $W = [w^c_k]$ is the weight matrix of the last dense layer in f, then the importance of each positional unit a_{ij} for the classification of label c can then be summarized as:

$$L^c_{\text{CAM}}(f,x) = \text{ReLU}(\sum_k w^c_k A^k) \tag{1}$$

In practice, L^c_{CAM} represents a visual signal of considerably smaller size when compared to the input image, and it is therefore resized to match the original sizes. This entails CAM will produce maps containing fairly imprecise object boundaries, when compared to gradient-based saliency methods. Furthermore, negative and zero values in the CAM are usually discarded through the application of the Rectified Linear Unit (ReLU) activation function. This is done by taking into consideration that these values either correspond to unrelated sections or sections that negatively contributes to the class of interest. Without this step, any normalization (commonly employed by visualization tools) over the map will nullify the most negative contributing regions, while sporadically highlighting unrelated regions.

Since then, a large spectrum of CAM-based methods have been developed. Gradient information was leveraged to extend CAM to Grad-CAM (Selvaraju et al., 2017), in order to explain more complex network architectures, not limited to convolutional networks ending in simple layers such as Softmax classifiers and linear regressors. Let $S_c = f(x)_c$ be the score attributed by the network for class c with respect to the input image x, and $\frac{\partial S_c}{\partial A^k_{ij}}$ be the partial derivative of the score S_c with respect to the pixel (i,j) in the activation map A^k, then:

$$L^c_{\text{Grad-CAM}}(f,x) = \text{ReLU}(\sum_k \sum_{ij} \frac{\partial S_c}{\partial A^k_{ij}} A^k) \tag{2}$$

Grad-CAM++ (Chattopadhay et al., 2018) was then proposed as an extension of Grad-CAM, in which each positional unit in A^k was weighted by leveling factors to produce maps that evenly highlighted different parts of the image that positively contributed to the classification of class c, providing a better cover for large objects and multiple instances of the same object in the image. Furthermore, the authors defined two metrics – Increase of Confidence (%IC) and Average Drop (%AD) – that have been constantly employed in the evaluation of visualization techniques.

More recently, it is noticeable an ever-growing interest in developing even more accurate visualization methods. Among many, we remark Score-CAM (Wang et al., 2020), Ablation-CAM (Ramaswamy et al., 2020) and Relevance-CAM (Lee et al., 2021). In the first, visualization maps are defined as the sum of the activation signals A^k, weighted by factors C^k, that are directly proportional to the classification score obtained when the image pixels are masked by the signal A^k itself. Ablation-CAM is similarly defined, as the sum of feature maps A^k, where each map is weighted by the proportional drop in classification score when A^k is set to zero. Finally, Relevance-CAM combines the ideas of Grad-CAM with Contrastive Layer-wise Relevance Propagation (CLRP) to obtain a high resolution explaining map that is sensitive to the target class. Notwithstanding their high accuracy, all of these methods entail large computing footprint.

While these methods together represent a consistent progression towards improving visualization results for single-class classification networks, little investigation has been conducted over the effectiveness of visualization techniques in multi-label scenarios, in which samples contain zero or multiple objects belonging to different labels at the same time. Additionally, studies that used multi-label datasets (Chattopadhay et al., 2018) often focus on single-label explanation, usually considering the highest scoring class as unit of interest. As motivation, we present the sample illustrated in Fig. 1, in which CAM-based methods (specially the most recent versions which attempt to expand the map to cover all parts of the classified object) seem to overflow the boundaries of the object of interest, even expanding over other objects associated with different labels.

We set forth the goal of analyzing the visualization techniques proposed so far in the multi-label setting, as well as developing a visualization technique which takes into account the expanded information available in multi-label problems. From the scientific and engineering perspective, the study of the multi-label scenario is interesting, as it allows for multiple objects to be present in a single sample, and thus requiring less constrained capturing conditions and pushing towards more reliable solutions. Furthermore, we observe a constantly increasing interest in weakly supervised segmentation (Chan et al., 2021) and localization (Zhang et al., 2021) problems, in which maps generated from CAM-based visualization strategies can be either used as pseudo ground-truth segmentation maps or leveraged to produce initial seed regions that are refined into full segmentation maps.

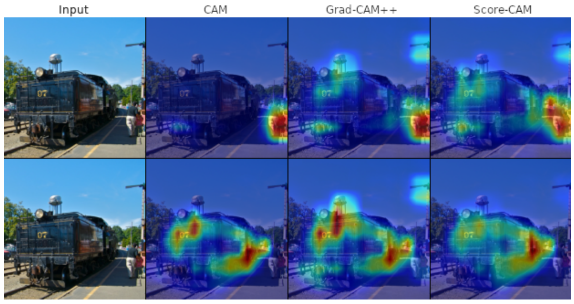

Figure 1: Application of CAM-based visual explaining methods over an image sample in the Pascal VOC 2007 validation dataset (Everingham et al., 2010). In the first row, CAM for label *person* slightly activate on top the object *train*. In the second row, CAM for *train* extends and overflow the boundaries of the objects.

3 PROPOSED APPROACH

In this section, we describe our approach to leveraging multi-label information into CAM. We start by describing the motivation and intuition behind it. We then formally define MinMax-Grad-CAM and MinMax-CAM, and, finally, present a variation that forms visualization maps by composing *positive*, *negative* and *background* contributions.

3.1 Intuition

A multi-label setting naturally entails more training complexity, as the visual pattern described associated with a present label does not need to be the most prominent visual cue in the sample. Statistical artifacts in the datasets, such as label co-occurrence and context, have great impact on the training of the model. For instance, if the correlation between two labels is 100%, then no concrete anchor between each label and its correct correct visual clues exist. In this case, it would be impossible to learn a consistent form to separate them (Chan et al., 2021). In the more reasonable scenario of two labels frequently appearing together (e.g., *dining table* and *chair* in Pascal VOC 2012 (Everingham et al., 2010)), we expect the network to take the occurrence of visual cues from one label into consideration when discriminating the other, possibly learning a false association which will ultimately translate into confusing CAMs and an increase the false positive rate of the labels.

We propose a visualization method that attempts to identify the kernel contributing regions for each label c in the input image x by averaging the signals in A^k, weighted by a combination of their direct contributions to the score of c and negative contributions to the remaining labels present in x, that is, finding regions that *maximize* the score of the label c and *minimize* the score of the remaining adjacent labels. To achieve this, we modify the gain function used by Grad-CAM to accommodate both maximizing and minimizing label groups, redefining it as the gradient of an optimization function J_c with respect to the activating signal A^k_{ij}, where J_c is the subtraction between the positive score for label c and the scores of the remaining labels represented within sample x.

3.2 Methodology

Let x be an input sample (image) from the set, associated with the set of labels C_x, f a trained convolutional network s.t. A^k is the activation map for the k-th kernel in the last convolutional layer of f, and $S_c = f(x)_c$ the score for the label of interest c. Furthermore, let $N_x = C_x \setminus \{c\}$. The focused score for label c is defined as:

$$J_c = S_c - \frac{1}{|N_x|}\sum_{n\in N_x} S_n \tag{3}$$

Then,

$$L^c_{\text{MinMax Grad-CAM}}(f,x) = \text{ReLU}(\sum_k \alpha^c_k A^k) \tag{4}$$

where

$$\alpha^c_k = \sum_{ij} \frac{\partial J_c}{\partial A^k_{ij}} \tag{5}$$

On the other hand, J_c is a linear function with respect to $S_k, \forall k \in C_x$:

$$\frac{\partial J_c}{\partial A^k_{ij}} = \frac{\partial S_c}{\partial A^k_{ij}} - \frac{1}{|N_x|}\sum_{n\in N_x} \frac{\partial S_n}{\partial A^k_{ij}} \tag{6}$$

Hence, MinMax Grad-CAM can be rewritten in its more efficient and direct "CAM form" (as demonstrated by Selvaraju et al. (Selvaraju et al., 2017)), for convolutional networks where the last layer is a linear classifier. In this form, Equation (5) simplifies to:

$$\alpha^c_k = w^u_k - \frac{1}{|N_x|}\sum_{n\in N_x} w^n_k \tag{7}$$

In conformity with the literature, we employ the ReLU activation function in both forms (CAM and Grad-CAM) to only retain regions that positively contribute to function J_c.

3.3 Distinguishing Positive, Negative and Background Regions

As a convolutional network is trained over a multi-label problem, the weights in the last *sigmoid* classifying layer will be adjusted to declare or refute the occurrence of a label according to the multiple patterns described in the signal $g^k = \text{GAP}(A^k_{ij})$.

If the ReLU activation function is used in the last convolutional layer, then g^k is a positive signal, and $\sum_{ij} \frac{\partial S_c}{\partial A^k_{ij}} > 0$ is invariably associated with kernels that positively contribute to the classification of label c. Conversely, $\sum_{ij} \frac{\partial S_c}{\partial A^k_{ij}} < 0$ indicate kernels that negatively affect the classification of c.

By naively subtracting contributions in Equations (3) and (7) and applying the ReLU activation function on top of the resulting CAM map, negative gradients from minimizing labels become positive, resulting in a map which highlights regions that positively contribute to the classification of label c, while presenting some residual activation on top of regions that negatively contribute to all adjacent labels being minimized. To overcome this artifact, we opted to decompose the contribution factors a^c_k into *positive*, *negative* and *overall negative* (which, in our experiments, frequently overlapped *background* regions). In this form, a^c_k is defined as:

$$\begin{aligned}\alpha^c_k = \sum_{ij}\Bigg[&\max\left(0, \frac{\partial S_c}{\partial A^k_{ij}}\right) \\ &- \frac{1}{|N_x|}\max\left(0, \sum_{n\in N_x}\frac{\partial S_n}{\partial A^k_{ij}}\right) \\ &+ \frac{1}{|C_x|}\min\left(0, \sum_{i\in C_x}\frac{\partial S_i}{\partial A^k_{ij}}\right)\Bigg]\end{aligned} \tag{8}$$

For the remaining of this article, we refer to this form as D-MinMax Grad-CAM. Finally, a CAM derivation is also possible:

$$\begin{aligned}\alpha^c_k = \Big[&\max(0, w^c_k) \\ &- \frac{1}{|N_x|}\max(0, \sum_{n\in N_x} w^n_k) \\ &+ \frac{1}{|C_x|}\min(0, \sum_{i\in C_x} w^i_k)\Big]\end{aligned} \tag{9}$$

4 EXPERIMENTAL SETUP

In this section, we detail the experimental settings used to compare the proposed strategy with the current visualization strategies found in the literature.

4.1 Datasets

To demonstrate that our results can be reproduced over different contexts, we test it over four distinct datasets. A brief summary of each is provided below.

4.1.1 Pascal VOC 2007

This set comprises 2,501 training samples, 2,510 validation samples and 4,952 test samples. Samples correspond to images with multiple objects belonging to 20 distinct classes (Everingham et al., 2010).

4.1.2 Pascal VOC 2012

Similar to Pascal VOC 2007, this version of the dataset comprises 5,717 training samples, 5,823 validation samples and 10,991 unlabeled test samples (Everingham et al., 2010).

4.1.3 COCO 2017

Image samples in this set contain multiple objects belonging to 80 distinct classes in their usual scenario, and present rich classification, detection and segmentation annotation (Lin et al., 2014). This version contains 118,287 training samples, 5,000 validation samples and 40,670 unlabeled test samples.

4.1.4 Planet: Understanding the Amazon from Space

This set comprises 40,479 training samples and 61,191 test samples (Shendryk et al., 2018). Samples correspond to satellite images from the Amazon rainforest, and are associated with one or more of the 17 distinct labels that classify human activity in the area.

4.2 Architectures and Training

To demonstrate the efficacy of our solution over different architectures, we have trained three distinct networks over Pascal VOC 2007: VGG16-GAP, ResNet101 and EfficientNet-B6. We approximate the evaluation conditions of previous works (Selvaraju et al., 2017; Chattopadhay et al., 2018; Wang et al., 2020) by warm-starting from weights pre-trained over the ILSVRC 2012 dataset, and fine tuning the networks over the Pascal VOC 2007 dataset (Everingham et al., 2010). Due to resource and time restrictions, we only experiment with the ResNet101 architecture over the remaining problem sets.

For each experiment, images in the observed sets are resized with the preservation of the aspect ration, such that their shortest dimension matches the expected size for the visual receptive field of the network. They are then centrally cropped to the exact size of the aforementioned field (224×224 for VGG-GAP and 512×512 for ResNet101 and EfficientNetB6). Visualization results are reported over the validation set, in conformity with literature.

Training is performed as follows: pre-trained weights are restored for the convolutional layers, a GAP and a *sigmoid* dense layer are added with the number of units equal to the number of labels in the dataset. All layers but the last are frozen (the gradient signal backpropagated during training is set to zero), and the model is trained for 30 epochs with a learning rate = 0.1. Approximately 60% of the layers (on the top) are then unfrozen and the model is once again trained for 80 epochs using Stochastic Gradient Descent with learning rate = 0.01 and Nesterov momentum = 0.9.

For both training stages, once a plateau is reached (defined as 3 epochs without validation loss decrease), learning rate is reduced by a factor of 0.5 and the best weights (yielding the lowest *validation loss*) found so far are restored. The early stopping mechanism triggers if validation loss does not decrease for 20 epochs.

4.3 Evaluation Metrics

We leverage the metrics defined by Chattopadhay et al. (Chattopadhay et al., 2018) to evaluate our results, but make slight alterations to them in order to accommodate multi-label problems. Specifically, *Increase in Confidence* (Equation (10)) and *Average Drop* (Equation (11)) take into consideration all labels in each image. We also present three new distinct metrics designed to evaluate the effect of the visualization maps over co-occurring labels, which are also listed below. Notice that, in a single-label classification setup, the equations below reduce to their conventional form, commonly described in the literature.

While we present the metrics in their *micro-average* form for simplicity, it is important to remark that this form does not capture well the unbalanced nature of multi-label problems (Tarekegn et al., 2021). To produce more reliable results, we report metrics in their *macro-averaged* form (or *class-frequency balanced*), in which class-specific metrics are computed separately and averaged regardless of label frequency.

4.3.1 Increase in Confidence (%IC)

The rate in which masking the input image x_i by the visualization mask M_i^c has produced a higher classification score $O_{ic}^c = f(M_i^c \circ x_i)^c$ than the baseline

$Y_i^c = f(x_i)^c$:

$$\frac{1}{\sum_i |C_i|} \sum_i^N \sum_{c \in C_i} [Y_i^c < O_{ic}^c] \tag{10}$$

This metric measures scenarios where removing background noise must improve classification confidence. We report results for this metric in compliance with literature, but raise the following question regarding the consistency of this metric: the classifying units of a *sigmoid* classifier are not in direct competition with each other for total activation energy, as it happens with units in *softmax* classifiers. For an ideal classifier, in which concepts are perfectly separated and no false correlation exist, one could argue that the removal of an object from an image should not affect the classification score of another object.

4.3.2 Average Drop (%AD)

The rate of drop in the confidence of a model for a particular image x_i and label c, when only the highlighted region $M_i^c \circ x_i$ is fed to the network:

$$\frac{1}{\sum_i |C_i|} \sum_i^N \sum_{c \in C_i} \frac{\max(0, Y_i^c - O_{ic}^c)}{Y_i^c} \tag{11}$$

Average Drop expresses the idea that masking the image with an accurate mask should not decrease confidence in the label of interest, that is, it measures if your mask is correctly positioned on top of the important regions that determine the label of interest.

4.3.3 Average Drop of Others (%ADO)

The rate of drop in the confidence of a model for a particular image x_i and labels $n \in N_i = C_i \setminus \{c\}$, when only the highlighted region $M_i^c \circ x_i$ is fed to the network:

$$\frac{1}{\sum_i |C_i|} \sum_i^N \sum_{c \in C_i} \frac{1}{|N_i|} \sum_{n \in N_i} \frac{\max(0, Y_i^n - O_{ic}^n)}{Y_i^n} \tag{12}$$

This metric captures the effect of a mask M_i^c over objects of other labels N_i present in x_i, in which the masking of the input x_i for a given class c should cause the confidence in other labels to drop. One expects an ideal mask to not retain any objects of other classes, that is, $f(M_i^c \circ x_i)^n \approx 0, \forall n \in N_i$.

4.3.4 Average Retention (%AR)

The rate of retention of confidence of a model for a particular image x_i and label c, when the region highlighted by the visualization map for label c is occluded:

$$\frac{1}{\sum_i |C_i|} \sum_i^N \sum_{c \in C_i} \frac{\max(0, Y_i^c - \bar{O}_{ic}^c)}{Y_i^c} \tag{13}$$

where $\bar{O}_{ic}^c = f((1 - M_i^c) \circ x_i)^c$.

While *Average Drop* measures if the map M_i^c is correctly positioned over an object of label c, *Average Retention* attempts to capture if M_i^c covers all regions occupied by objects of label c, that is, masking the input with an accurate complement mask $(1 - M_i^c)$ should decrease confidence in class c.

4.3.5 Average Retention of Others (%ARO)

The rate of retention of confidence of a model for a particular image x_i and labels $n \in N_i$, when the region highlighted by the visualization map for label c is occluded:

$$\frac{1}{\sum_i |C_i|} \sum_i^N \sum_{c \in C_i} \frac{1}{|N_i|} \sum_{n \in N_i} \frac{\max(0, Y_i^n - \bar{O}_{ic}^n)}{Y_i^n} \tag{14}$$

This metric evaluates if the masking of input x_i for all labels but c retains the confidence of the model in detecting these same labels. An ideal mask complement for class c should cover all objects of the other classes, that is, $f((1 - M_i^c) \circ x_i)^n \approx f(x_i)^n, \forall n \in N_i$.

4.3.6 F_1- and F_1+ Scores

While the previously described metrics cover many aspects of the application of visualization techniques over multi-label problems, it is not ideal or practical to keep track of multiple scores at once. Hence, we opted to summarize similar metrics using the harmonic mean (or F_1 score). More specifically, we consider (a) F_1-: the harmonic mean between *Average Drop* and *Average Retention of Others*, both error minimizing metrics, in which low is better; and (b) F_1+: the harmonic mean between *Average Retention* and *Average Drop of Others*, both gain maximizing metrics, in which high is better.

5 RESULTS

In this section, we present both quantitative and qualitative results for MinMax-CAM and D-MinMax-CAM, as well as for other well established explaining techniques found in the literature. We then discuss the properties and limitations of our technique.

5.1 Quantitative Results

Table 1 lists the metrics detailed in Section 4.3 over Pascal VOC 2007 validation set, considering the EfficientNet-B6 (Eb6), ResNet-101 (RN101) and VGG16-GAP (VGG16) architectures. Grad-CAM++

and Score-CAM display the highest *Increase in Confidence* (%IC) for most architectures (two out of three). For EfficientNet-B6, CAM obtained the highest value for this metric (39.67%), closely followed by D-MinMax-CAM (a difference of 0.18 percent points). For the remaining architectures, MinMax-CAM and D-MinMax-CAM present slightly lower %IC than CAM.

CAM, Grad-CAM++ and Score-CAM achieve the best *Average Drop* (%AR) and *Average Retention* (%AD) scores, as these metrics favor methods producing diffuse activation maps. More specifically: Grad-CAM++ and Score-CAM obtained a significantly lower %AD compared to the others, while CAM obtained marginally higher %AR scores than MinMax. Conversely, MinMax-CAM and D-MinMax-CAM consistently achieve better results for %ADO and %ARO, as these metrics favor methods that produce more focused maps.

When considering the aggregated metric F_1-, MinMax-CAM and D-MinMax-CAM show much better score results than CAM and Grad-CAM++. This indicates that they are quite successful at removing regions containing objects of adjacent labels $n \in N_x$, while still focusing on determinant regions for the classification of c. For the ResNet101 architecture, MinMax and D-MinMax-CAM scored very closely to the winner Score-CAM (0.01 percent points difference).

CAM and MinMax-CAM present very close results in F_1+ score (closely followed by D-MinMax-CAM), while Grad-CAM++ and Score-CAM techniques produced lower scores for this metric. This indicates that CAM, MinMax-CAM and D-MinMax-CAM are more successful in covering large portions of objects of label c without spreading over objects of adjacent labels than Grad-CAM++ and Score-CAM.

Results for multiple datasets (shown in Table 2) shows similar values for the three metrics. Once again, CAM, Grad-CAM++ and Score-CAM produce the best %IC, %AD and %AR values. We attribute this to the proclivity of these techniques to retain large portions of the image, maintaining contextual information of the sample. Conversely, D-MinMax-CAM wins against the literature techniques by a large margin when considering %ADO, %ARO and F_1- score. Finally, CAM and MinMax-CAM present similar results for F_1+ score, consistently ahead of Grad-CAM++ and Score-CAM.

With respect to evaluation performance, no significant difference was observed between CAM, Grad-CAM++, MinMax-CAM and D-MinMax-CAM; as all methods could be evaluated under 30 minutes over the different datasets. On the other hand, Score-CAM

Table 1: Report of metric scores per method, considering multiple architectures over the Pascal VOC 2007 dataset.

Metric	Model	CAM	Grad-CAM++	Score-CAM	MinMax-CAM	D-MinMax-CAM
%IC	Eb6	**39.67%**	25.13%	30.50%	34.23%	39.49%
	RN101	27.68%	31.03%	**40.76%**	26.61%	23.83%
	VGG16	5.65%	8.27%	**12.78%**	4.18%	3.76%
%AD	Eb6	22.94%	36.87%	**22.10%**	28.09%	23.71%
	RN101	25.24%	17.90%	**10.79%**	32.58%	39.25%
	VGG16	39.34%	29.22%	**19.27%**	46.78%	50.34%
%ADO	Eb6	29.43%	19.35%	20.17%	**39.82%**	31.99%
	RN101	32.73%	12.48%	14.72%	44.03%	**46.49%**
	VGG16	29.61%	18.52%	15.74%	39.33%	**39.50%**
%AR	Eb6	**11.74%**	8.40%	9.92%	10.50%	9.10%
	RN101	**16.54%**	14.04%	14.94%	14.27%	12.00%
	VGG16	40.38%	39.04%	**42.70%**	33.82%	31.00%
%ARO	Eb6	1.61%	2.53%	2.28%	**0.99%**	1.47%
	RN101	2.44%	3.94%	3.43%	1.28%	**1.16%**
	VGG16	8.84%	12.10%	12.96%	3.47%	**3.34%**
F_1-	Eb6	2.82%	4.54%	1.91%	**1.86%**	2.64%
	RN101	4.05%	5.62%	**2.20%**	2.38%	2.21%
	VGG16	13.52%	15.39%	13.42%	6.23%	**6.00%**
F_1+	Eb6	**15.79%**	10.14%	5.96%	15.40%	12.96%
	RN101	**20.84%**	11.97%	6.89%	19.85%	17.13%
	VGG16	31.70%	23.50%	22.19%	**32.16%**	29.94%

Table 2: Report of metric scores per method, over multiple datasets.

Metric	Dataset	CAM	Grad-CAM++	Score-CAM	MinMax-CAM	D-MinMax-CAM
%IC	P:AfS	6.09%	7.05%	**11.59%**	6.22%	6.27%
	COCO	30.21%	32.98%	**44.69%**	23.12%	19.20%
	VOC07	27.68%	31.03%	**40.76%**	26.61%	23.83%
	VOC12	27.75%	25.40%	**35.10%**	24.70%	21.66%
%AD	P:AfS	55.25%	49.00%	**43.37%**	64.24%	66.88%
	COCO	27.42%	17.56%	**9.62%**	40.22%	47.43%
	VOC07	25.24%	17.90%	**10.79%**	32.58%	39.25%
	VOC12	24.47%	18.69%	**10.60%**	29.17%	34.22%
%ADO	P:AfS	43.61%	33.67%	34.06%	60.04%	**60.62%**
	COCO	51.49%	20.59%	24.45%	68.04%	**71.90%**
	VOC07	32.73%	12.48%	14.72%	44.03%	**46.49%**
	VOC12	36.44%	14.92%	18.46%	43.65%	**45.02%**
%AR	P:AfS	46.42%	**49.45%**	48.01%	37.16%	32.74%
	COCO	**27.70%**	25.60%	26.64%	24.44%	22.79%
	VOC07	**16.54%**	14.04%	14.94%	14.27%	12.00%
	VOC12	**16.23%**	14.71%	16.22%	14.60%	13.06%
%ARO	P:AfS	25.48%	29.46%	28.13%	20.84%	**18.55%**
	COCO	5.26%	7.92%	7.71%	3.31%	**3.13%**
	VOC07	2.44%	3.94%	3.43%	1.28%	**1.16%**
	VOC12	2.29%	3.76%	3.32%	1.21%	**1.14%**
F_1-	P:AfS	30.68%	32.07%	28.46%	28.35%	**26.42%**
	COCO	8.23%	9.94%	7.39%	5.82%	**5.64%**
	VOC07	4.05%	5.62%	**2.20%**	2.38%	2.21%
	VOC12	3.89%	5.70%	4.30%	2.26%	**2.17%**
F_1+	P:AfS	39.54%	35.11%	35.41%	**41.00%**	37.01%
	COCO	34.05%	21.45%	23.82%	**34.07%**	32.44%
	VOC07	**20.84%**	11.97%	6.89%	19.85%	17.13%
	VOC12	**21.25%**	13.87%	16.39%	20.25%	18.60%

took approximately 16 hours, 59 hours and 29 hours to be evaluated over Pascal VOC 2007, Pascal VOC 2012 and Planet: Understanding the Amazon from Space datasets, respectively.

5.2 Considerations and Limitations

Fig. 2 and Fig. 3 illustrate the application of each visualization technique over a few samples in the Pascal VOC 2012 and VOC 2007 datasets, respectively. Grad-CAM++ and Score-CAM seem to generate more diffused maps, that overflow the boundaries of the object of interest and even cover large portions of the scenario. On the other hand, MinMax-CAM produces more focused activation maps by avoiding adjacent objects from different labels, while D-MinMax-CAM reduces residual activation over the scenario by filtering background contribution.

MinMax-CAM works under the assumption that two distinct labels are not associated with the same set of visual cues present in a single region in the input image. Hence, the contributions being subtracted are associated with different parts of the spatial signal A^k, and the resulting map is more focused than its counterpart generated by CAM. This assumption does not hold when a network has not learned sufficiently discriminative patterns for both labels, which can be caused by an unbalanced set or a subset of frequently co-occurring labels (Chan et al., 2021). For instance, *tv monitors* frequently appear together with *chairs* in Pascal VOC 2007, which might teach the network to correlate the occurrence of the latter with the classification of a former. In such scenarios, MinMax-CAM could degenerate the explanation map (Fig. 4a).

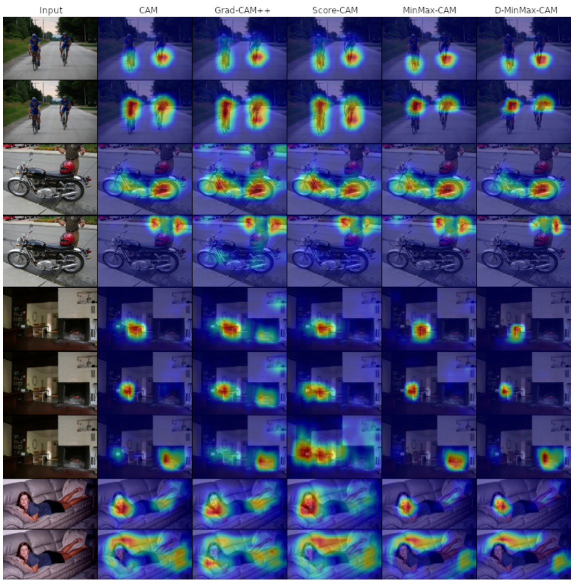

Figure 2: Comparison between CAM-based visualization techniques over Pascal VOC 2012 dataset. Labels being explained are, from top to bottom: *bicycle*, *person*, *motorbike*, *person*, *dining table*, *chair*, *tv monitor*, *person* and *sofa*.

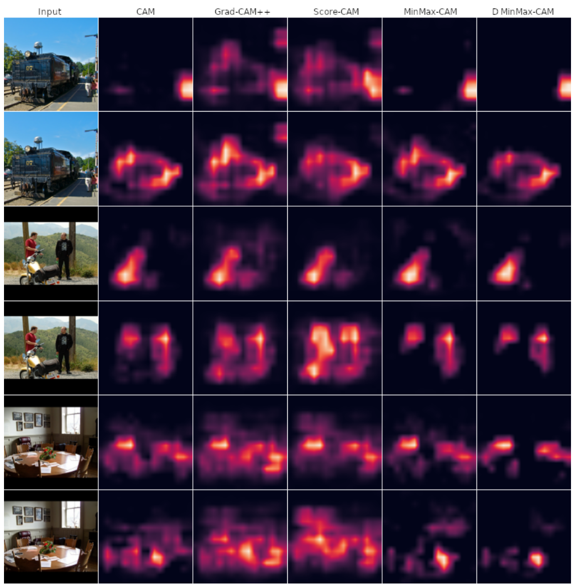

Figure 3: Comparison between CAM-based visualization techniques over Pascal VOC 2007 dataset. Masks are shown instead of overlays in order to facilitate visual inspection. The labels being explained are, from top to bottom: *person*, *train*, *motorbike*, *person*, *chair*, and *dining table*.

6 IMPROVING VISUALIZATION

While label co-occurrence information might be useful from the classification perspective, handing clues about the context to the classifier, it provokes unexpected highlighting in regions that do not contain the label. One obvious way to overcome this is to encourage solutions that more clearly separate labels and penalizing the ones that rely on label co-occurrence information. In this vein, Chan et al. studied the effect of “balancing” the class distribution of the DeepGlobe dataset over weakly supervised segmentation, by removing samples with frequently co-occurring labels, and achieved mixed results (Chan et al., 2021); while Su et al. proposed a context decoupling strategy based on augmenting samples by pasting objects outside their usual context (Su et al., 2021).

We propose a regularization strategy that encourages the formation of a positive and sparse synaptic connection between the signal $g = \text{GAP}(A_{ij}) \in \mathbb{R}^k$ (the output of the last convolutional layer) and the classifying *sigmoid* layer. Intuitively, if the presence of a pattern g^k is strongly associated with the classification of a given label c, then g^k should not be used in the decision process of the other labels $n = C_x \setminus \{c\}$ (e.g., the presence of a *dining table* should not contribute to the classification of a *chair*). Furthermore, we penalize negative connection values in order to focus on visual patterns that do characterize the label, instead of contextual information which indicates its probable absence (e.g., the absence of a *dining table* should not imply absence of *chairs*).

6.1 Kernel Usage Regularization

Let k be the number of kernels in the last convolutional layer, l be the number of labels in the dataset, $g = [g^i]_k$ be the feature vector obtained from the pooling of last convolutional layer, $W = [w_i^c]_{k\times l}$ and $b = [b_c]_l$ the weights from the last dense layer and σ the *sigmoid* function. Then, the *sigmoid* classifier can be regularized as follows:

$$\begin{aligned} W^r &= W \circ \text{softmax}(W) \\ y &= \sigma(g \cdot W^r + b) \end{aligned} \tag{15}$$

It is possible to observe that the simple application of the *softmax* function over each row in the matrix W summarizes all of the desired aspects of the regularization: large values w_i^c (indicating strong connection between the matching of the pattern described by kernel i and the classification of label c) will induce $softmax(w_{i\_})^c \approx 1$, and thus $w_i^{c^r} \approx w_i^c$. As the *softmax* function quickly saturates over a few large values, it will push the remaining connections towards 0 (erasing the influence kernel i has over the classification of other labels). Finally, very low (negative) values w_{ij} should have low $softmax(w_{i\_})^c$, implying $w_i^{c^r} \approx 0$.

Fig. 4b illustrates the activation maps for the network trained with regularized weights. As the simultaneous usage of same kernels for distinct classification units have been regularized, subtracting contributions no longer distort the maps for any of the labels.

6.2 Results

To demonstrate the efficacy of this strategy, we train regularized versions of ResNet101 network and compare them with their unregularized counterparts.

In each experiment, we inspected (a) the weight histograms for each classifying unit in the last layer; (b) the correlation matrix between the weight vectors obtained from each unit; and (c) the top-10 most contributing kernels for each of the aforementioned units. We concluded that (a) most weights have become positive, as the histograms shifted from a normal-like distribution centered in zero to a right-skewed-like distribution; (b) units present a much lower correlation with each other than the ones observed in their non-regularized counterparts; and (c) units shared significantly less top-10 most contributing kernels.

Table 3 shows the visualization results over multiple datasets, using a ResNet101 network with a regularized *sigmoid* classifier. Once again, Grad-CAM++ and Score-CAM present high values for %IC. D-MinMax-CAM shows the best F_1- scores in all datasets but one, staying in third place with a difference of 0.53 percent points from the winner (Score-CAM). Finally, MinMax-CAM and D-MinMax-CAM showed the best results in 3 out of 4 tests for the F_1+ score, while achieving a similar score to the winner (CAM) of the last test (VOC 2007). We observe an overall increase in both *Increase in Confidence* and F_1+ score for most CAM techniques and datasets, when compared with their unregularized counterparts. On the other hand, re-

Table 3: Report of metric scores over multiple datasets, per method. Models were regularized during training.

Metric	Dataset	CAM	Grad-CAM++	Score-CAM	MinMax-CAM	D-MinMax-CAM
%IC	P:AfS	**15.60%**	14.39%	14.13%	11.43%	11.54%
	COCO	34.43%	36.81%	**37.87%**	21.47%	21.49%
	VOC07	28.71%	28.07%	**34.93%**	23.90%	24.99%
	VOC12	33.32%	34.90%	**37.30%**	29.54%	29.36%
%AD	P:AfS	42.51%	42.67%	**39.50%**	51.96%	52.53%
	COCO	22.52%	19.86%	**13.91%**	41.29%	41.39%
	VOC07	22.89%	18.65%	**11.69%**	29.80%	34.19%
	VOC12	16.09%	15.32%	**10.46%**	22.22%	22.85%
%ADO	P:AfS	38.34%	35.46%	35.21%	**49.58%**	49.51%
	COCO	46.97%	37.63%	25.57%	69.17%	**69.28%**
	VOC07	37.30%	20.06%	17.27%	47.16%	**48.60%**
	VOC12	29.66%	21.89%	15.95%	42.07%	**42.46%**
%AR	P:AfS	**47.28%**	46.50%	43.61%	43.17%	43.01%
	COCO	**34.40%**	34.21%	28.13%	30.05%	30.04%
	VOC07	**18.64%**	17.35%	16.91%	16.02%	14.72%
	VOC12	**18.66%**	18.37%	17.72%	17.10%	16.99%
%ARO	P:AfS	25.43%	26.35%	26.80%	20.79%	**20.72%**
	COCO	7.14%	7.85%	11.36%	4.24%	**4.23%**
	VOC07	2.44%	3.45%	3.95%	1.35%	**1.22%**
	VOC12	2.59%	2.89%	4.00%	1.22%	**1.20%**
F_1-	P:AfS	27.02%	27.68%	**26.62%**	26.86%	27.15%
	COCO	10.08%	10.38%	11.15%	**7.33%**	**7.33%**
	VOC07	4.12%	5.41%	2.69%	2.47%	**2.28%**
	VOC12	3.97%	4.30%	4.96%	2.24%	**2.21%**
F_1+	P:AfS	36.53%	35.05%	34.46%	**39.15%**	39.03%
	COCO	38.08%	34.42%	25.19%	40.64%	**40.65%**
	VOC07	**23.89%**	17.87%	8.10%	22.38%	20.97%
	VOC12	21.99%	19.28%	16.24%	**22.84%**	22.78%

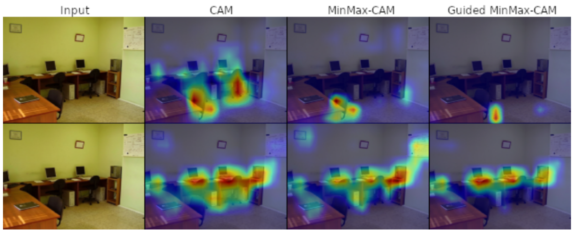

(a)

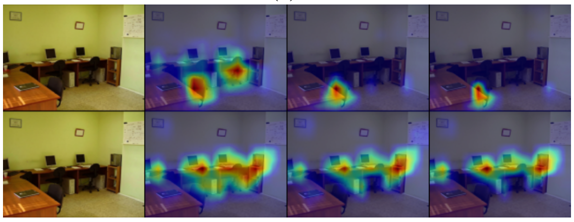

(b)

Figure 4: (a) Degenerated example in Pascal VOC 2007, in which contributing regions for the detection of label *chair* collide with the ones for label *tv monitor*. (b) Activation maps after the network is trained with regularized weights.

sults for F_1- score were mixed: the value for this metric has decreased in 9 out of 18 tests. Furthermore, we notice very similar results from both MinMax-CAM and D-MinMax-CAM in all metrics and datasets. This can be attributed to the regularization factor, which penalizes the existence of negative weights, approximating $\max(0, w_k^c)$ to w_k^c and, thus, D-MinMax-CAM to MinMax-CAM.

Table 4 reports the F_1 and F_2 scores over validation and test sets (when available) for both baseline and regularized models. We see a slight increase in F_1 and F_2 score in most cases, indicating that this regularization has positive impact on overall score of the classifier. Conversely, an unexpected decrease in score was observed for COCO 2017, which might be associated with its high number of labels and the training settings used. We hypothesize that a careful tune of hyperparameters (such as *learning rate*) can achieved better results, given the aggressively sparse nature of this regularization strategy.

Table 4: Multi-label classification score over multiple datasets, considering the baseline and regularized (Reg.) models.

Metric	Dataset	Baseline	Reg.
F_2	P:AfS Val	87.80%	**88.24%**
F_2	P:AfS Priv. Test	89.22%	**89.81%**
F_2	P:AfS Public Test	89.62%	**90.10%**
F_1	COCO 2017 Val	**75.64%**	74.23%
F_1	VOC 2007 Test	84.26%	**85.85%**
F_1	VOC 2012 Val	85.05%	**85.90%**

7 CONCLUSIONS

In this work, we promoted an analysis for visualization techniques over multi-label scenarios. We proposed generalizations of the well-known *Increase in Confidence* and *Average Drop* metrics, accounting for the multiple labels within each sample, and presented three new metrics that capture the effectiveness of visualization maps in images containing objects of distinct labels. We found existing techniques, focused solely on optimizing *Increase in Confidence* and *Average Drop*, to produce diffuse maps.

We presented a visualization technique that produces visualization maps considering the activation maximization for a labels of interest while minimizing the activation of adjacent labels. We further refined this technique by decomposing it into *positive*, *negative* and *background* contributions in order to produce cleaner visualization maps with minimal contextual residue. We tested our solutions over different datasets and architectures, obtaining encouraging results from the multiple metrics while maintaining low processing footprint (compared to the massively time consuming Score-CAM).

Finally, we proposed a regularization strategy which penalizes the usage of label co-occurrence information in the classification process by reinforcing positive and sparse weights in the classification layer. Quantitative results suggest that this strategy is effective in creating cleaner visualization maps while promoting better classification scores in most datasets.

Future work will include an evaluation of our technique over localization and weakly supervised segmentation problems, as well as the development of a generalized kernel usage regularization strategy that can extended to intermediate layers. Furthermore, we intent to study new ways to decouple label contextual information by distilling label-specific knowledge.

ACKNOWLEDGEMENTS

The authors would like to thank CNPq (grants 140929/2021-5 and 309330/2018-1) and LNCC/MCTI for providing HPC resources of the SDumont supercomputer.

REFERENCES

Adebayo, J., Gilmer, J., Muelly, M., Goodfellow, I., Hardt, M., and Kim, B. (2018). Sanity checks for saliency maps. In *32nd International Conference on Neural Information Processing Systems (NIPS)*, page

9525–9536, Red Hook, NY, USA. Curran Associates Inc.

Chan, L., Hosseini, M. S., and Plataniotis, K. N. (2021). A comprehensive analysis of weakly-supervised semantic segmentation in different image domains. *International Journal of Computer Vision (IJCV)*, 129(2):361–384.

Chattopadhay, A., Sarkar, A., Howlader, P., and Balasubramanian, V. N. (2018). Grad-CAM++: Generalized gradient-based visual explanations for deep convolutional networks. In *IEEE Winter Conference on Applications of Computer Vision (WACV)*, pages 839–847. IEEE.

Dhillon, A. and Verma, G. K. (2020). Convolutional neural network: a review of models, methodologies and applications to object detection. *Progress in Artificial Intelligence*, 9(2):85–112.

Everingham, M., Van Gool, L., Williams, C. K., Winn, J., and Zisserman, A. (2010). The pascal visual object classes (voc) challenge. *International Journal of Computer Vision (IJCV)*, 88(2):303–338.

Huff, D. T., Weisman, A. J., and Jeraj, R. (2021). Interpretation and visualization techniques for deep learning models in medical imaging. *Physics in Medicine & Biology*, 66(4):04TR01.

Lee, J. R., Kim, S., Park, I., Eo, T., and Hwang, D. (2021). Relevance-CAM: Your model already knows where to look. In *IEEE/CVF Conference on Computer Vision and Pattern Recognition (CVPR)*, pages 14944–14953.

Lin, T.-Y., Maire, M., Belongie, S., Hays, J., Perona, P., Ramanan, D., Dollár, P., and Zitnick, C. L. (2014). Microsoft coco: Common objects in context. In Fleet, D., Pajdla, T., Schiele, B., and Tuytelaars, T., editors, *European Conference on Computer Vision (ECCV)*, pages 740–755, Cham. Springer International Publishing.

Minaee, S., Boykov, Y. Y., Porikli, F., Plaza, A. J., Kehtarnavaz, N., and Terzopoulos, D. (2021). Image segmentation using deep learning: A survey. *IEEE Transactions on Pattern Analysis and Machine Intelligence (PAMI)*, pages 1–1.

Pons, J., Slizovskaia, O., Gong, R., Gómez, E., and Serra, X. (2017). Timbre analysis of music audio signals with convolutional neural networks. In *25th European Signal Processing Conference (EUSIPCO)*, pages 2744–2748. IEEE.

Ramaswamy, H. G. et al. (2020). Ablation-CAM: Visual explanations for deep convolutional network via gradient-free localization. In *IEEE/CVF Winter Conference on Applications of Computer Vision (WACV)*, pages 983–991.

Rawat, W. and Wang, Z. (2017). Deep convolutional neural networks for image classification: A comprehensive review. *Neural Computation*, 29(9):2352–2449.

Selvaraju, R. R., Cogswell, M., Das, A., Vedantam, R., Parikh, D., and Batra, D. (2017). Grad-CAM: Visual explanations from deep networks via gradient-based localization. In *IEEE International Conference on Computer Vision (ICCV)*, pages 618–626.

Shendryk, I., Rist, Y., Lucas, R., Thorburn, P., and Ticehurst, C. (2018). Deep learning - a new approach for multi-label scene classification in planetscope and sentinel-2 imagery. In *IEEE International Geoscience and Remote Sensing Symposium (IGARSS)*, pages 1116–1119.

Simonyan, K., Vedaldi, A., and Zisserman, A. (2014). Deep inside convolutional networks: Visualising image classification models and saliency maps. *CoRR*, abs/1312.6034.

Smilkov, D., Thorat, N., Kim, B., Viégas, F. B., and Wattenberg, M. (2017). SmoothGrad: removing noise by adding noise. *ArXiv*, abs/1706.03825.

Springenberg, J., Dosovitskiy, A., Brox, T., and Riedmiller, M. (2015). Striving for simplicity: The all convolutional net. In *International Conference on Learning Representations (ICLR) - Workshop Track*.

Srinivas, S. and Fleuret, F. (2019). Full-gradient representation for neural network visualization. *arXiv preprint arXiv:1905.00780*.

Su, Y., Sun, R., Lin, G., and Wu, Q. (2021). Context decoupling augmentation for weakly supervised semantic segmentation. *ArXiv*, abs/2103.01795.

Tachibana, H., Uenoyama, K., and Aihara, S. (2018). Efficiently trainable text-to-speech system based on deep convolutional networks with guided attention. In *IEEE International Conference on Acoustics, Speech and Signal Processing (ICASSP)*, pages 4784–4788.

Tarekegn, A. N., Giacobini, M., and Michalak, K. (2021). A review of methods for imbalanced multi-label classification. *Pattern Recognition*, 118:107965.

Wang, H., Wang, Z., Du, M., Yang, F., Zhang, Z., Ding, S., Mardziel, P., and Hu, X. (2020). Score-CAM: Score-weighted visual explanations for convolutional neural networks. *IEEE/CVF Conference on Computer Vision and Pattern Recognition Workshops (CVPRW)*, pages 111–119.

Wei, S.-E., Ramakrishna, V., Kanade, T., and Sheikh, Y. (2016). Convolutional pose machines. In *IEEE conference on Computer Vision and Pattern Recognition (CVPR)*, pages 4724–4732.

Yao, L., Mao, C., and Luo, Y. (2019). Graph convolutional networks for text classification. In *AAAI conference on artificial intelligence*, volume 33, pages 7370–7377.

Zhang, D., Han, J., Cheng, G., and Yang, M.-H. (2021). Weakly supervised object localization and detection: A survey. *IEEE Transactions on Pattern Analysis and Machine Intelligence*, pages 1–1.

Zhou, B., Khosla, A., Lapedriza, A., Oliva, A., and Torralba, A. (2016). Learning deep features for discriminative localization. In *IEEE Conference on Computer Vision and Pattern Recognition (CVPR)*, pages 2921–2929.